中国科技论文在线 http://www.paper.edu.cn

Design and analysis of all-optical XOR gate using SOA-based Mach–Zehnder interferometer

Min Zhang[a,*], Yongpeng Zhao[b], Ling Wang[a], Jian Wang[a], Peida Ye[a]

[a] *Optical Communication Center, Beijing University of Posts and Telecommunications, P.O. Box 125, Beijing 100876, PR China*
[b] *Electro-Optical Telecommunications Group, Department of Electrical Engineering, Eindhoven University of Technology, Eindhoven, The Netherlands*

Received 7 December 2002; received in revised form 9 May 2003; accepted 20 June 2003

Abstract

The performance of ultra-fast all-optical XOR gate using two types semiconductor optical amplifier-based Mach–Zehnder interferometers (SOA-MZIs) is analyzed. Key parameters are optimized through numerical simulations. With properly designed parameters, 40 Gb/s all-optical XOR gate using SOA-MZI can be realized with fairly high performance. The results are helpful for parameter design of SOA-MZI-based XOR gate.
© 2003 Published by Elsevier B.V.

PACS: 84.40.Ua; 42.79.Ta

Keywords: Optical communications; All-optical logic devices; All-optical XOR operation; Mach–Zehnder interferometer; Semiconductor optical amplifiers

1. Introduction

All-optical logic devices are vital elements in ultra-high speed all-optical networks. Particularly, optical Boolean XOR operation is indispensable to critical networking functions, such as switching, signal regeneration, address and header recognition, as well as data encoding and encryption.

Various schemes of all-optical XOR operation have been reported, such as 100 Gb/s XOR using the nonlinear optical loop mirror (NOLM) [1], XOR using terahertz optical asymmetric demultiplexer (TOAD) [2], 10 Gb/s XOR using SOA-based fiber Sagnac interferometer [3], 40 Gb/s XOR using ultra-fast nonlinear interferometer (UNI) [4], and 20 Gb/s XOR using interferometric wavelength converter (IWC) [5]. Given that devices exploiting semiconductor optical amplifier-based Mach–Zehnder interferometer (SOA-MZI) possess the practical advantages of low power consumption, low latency, high stability and integration potential, XOR gates of this type has been demonstrated [6]. However, by far, these demonstrations are restricted to 20 Gb/s and few studies have been made to analysis of the gate performance systematically. This paper aims to investigate the

* Corresponding author. Tel.: +8610-62282205; fax: +8610-62285008.
E-mail address: zmight@hotmail.com (M. Zhang).

0030-4018/$ - see front matter © 2003 Published by Elsevier B.V.
doi:10.1016/S0030-4018(03)01692-4

中国科技论文在线 http://www.paper.edu.cn

performance of SOA-MZI-based XOR gate at 20 Gb/s and above. Key parameters are optimized through numerical analysis and simulations. Besides, the data-pattern dependence of the gate and the speed limit are discussed.

2. Operation principle

The optical XOR gate in our study consists of a symmetrical MZI with one SOA located in the same relative position of each arm, as shown in Fig. 1. For the Boolean calculation $A \oplus B = C$, the input logic signals, A and B, enter the arms of the MZI via two multiplexers, respectively, functioning as the control signals. A clock stream enters Port 1 and splits into two equal parts via coupler C1, acting as the probe signals. In Fig. 1, the control and the probe pulses counter-propagate along both the arms, we call it colliding pulse MZI (CMZI). In case that the control and the probe pulses co-propagate, we call it traveling pulse MZI (TMZI). If the control signals A and B are identical, the SOA-MZI is balanced and no signal emerges from Port 3. In contrast, if one of the control signals is ZERO while the other is ONE, due to the cross-phase modulation (XPM) effect in the SOAs, a differential phase-shift is introduced briefly to these two probe signals so as to switch them out of Port 3. Thus, signal C at Port 3 is actually the result of Boolean calculation $A \oplus B$.

In the above configuration, we input the clock pulses as the probe signal, instead of a continuous-wave (CW) light. Thus the XOR gate is capable of all-optical 3R function with a higher extinction ratio [7]. Particularly, we pay more attention to CMZI in this study, for which a filter is unnecessary at Port 3 to reject the control signals and thus the device is more compact.

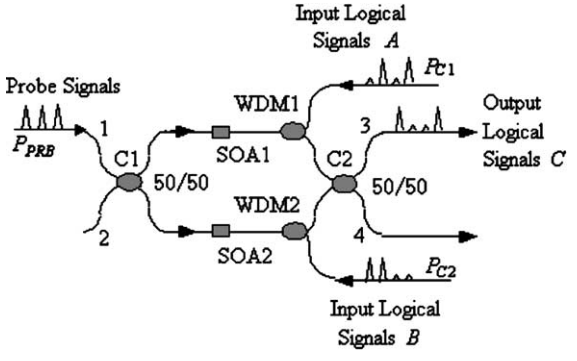


Fig. 1. Configuration of all-optical XOR gate using SOA-MZI.

For simplicity, we neglect the loss and the amplified spontaneous emission (ASE) noise in SOA. Also, we neglect the group velocity dispersion since its effect on the pulse propagation is negligible along the SOA length (several hundreds of micrometers). Thus the clock and the control signals travel through the SOA at the same speed. We assume the control signals and the clock have already been synchronized, the initial pulse phase in each arm is zero, and both SOAs are identical. If there is polarization effect, switching will happen even when both control signals are ONE or ZERO. We do not take the polarization-dependent effect into account by assuming both SOAs are polarization independent, both control signals have the same polarization and the relative polarization is maintained as they traverse the arms.

Thereafter, we define the pulse transmission time in the SOAs as $T_{\mathrm{TRAN}} = Ln_{\mathrm{SOA}}/c$, where n_{SOA} is the effective index of the SOAs. When T_{TRAN} is comparable to the pulse-width, as in this paper, the SOA length (L) and the nonlinear gain compression effect must be taken into consideration.

The generic gain and phase dynamic response of SOA under picosecond control pulses has already been studied in [8]. More accurate theoretical models have been discussed in [9,10]. However, since the input pulse energy is less than 1 pJ in this paper, we treat the SOAs with a simplified model by J.M. Tang, which does not include the effects of two-photon absorption (TPA) and ultrafast nonlinear refraction (UNR), as follows [11]:

$$\frac{\partial g_i(z,t)}{\partial t} = \frac{g_0 - g_i(z,t)}{\tau_{\mathrm{C}}} - \frac{g_i(z,t)}{1 + \varepsilon P_{\mathrm{C}i}(z,t)} \frac{P_{\mathrm{C}i}(z,t)}{E_{\mathrm{sat}}}, \tag{1}$$

$$\frac{\partial P_{\mathrm{C}i}(z,t)}{\partial z} = \frac{g_i(z,t)}{1 + \varepsilon P_{\mathrm{C}i}(z,t)} P_{\mathrm{C}i}(z,t), \tag{2}$$

$$\frac{\partial \phi_{\mathrm{C}i}(z,t)}{\partial z} = \frac{1}{2}\alpha \frac{g_i(z,t)}{1 + \varepsilon P_{\mathrm{C}i}(z,t)}, \tag{3}$$

中国科技论文在线 http://www.paper.edu.cn

where $P_{Ci}(zt))$ and $\phi_{Ci}(zt))$ $(i = 1, 2)$ are the power and the phase-shift of the control signals in the upper and the lower arms, respectively. g_0 is the small signal gain. τ_C is the spontaneous carrier lifetime. α is the linewidth enhancement factor. ε is the nonlinear gain compression factor due to the effect of carrier heating and spectral hole-burning. $g_i(zt))$ corresponds to the instant gain coefficient at a place (z) of the SOAs. E_{sat} is the saturation energy and satisfies

$$E_{sat} = P_{sat} \cdot \tau_C = \frac{\hbar\omega_0}{a_N} \cdot \frac{dW}{\Gamma}, \tag{4}$$

where h is the Plank constant, ω_0 is the control pulse center wavelength, a_N is the general gain factor, d and W are the depth and the width of the SOA active region, and Γ is the general confinement factor.

To modeling the characteristics for both co- and counter-propagation of the control signals with respect to the probe clock, we design the probe clock intensity so small as not to modify the optical properties of the SOAs, and take the transparency assumption similar to the approaches in [12,13]. Namely, the SOA is quasi-transparent to both the control pulse and the gain coefficient. The instant gain coefficients (h_i), the integral SOA gains (G_i) and the pulse phase-shifts ($\Delta\phi_i$) for both co- and counter-propagation in both arms are expressed as:

$$h_i(t) = \int_{-\infty}^{\infty} d\tau \int_{-L/2}^{L/2} g_i(z,\tau)\delta(\tau - t \pm zn_{SOA}/c)\,dz, \tag{5}$$

$$G_i(t) = \exp[h_i(t)], \tag{6}$$

$$\Delta\phi_i(t) = -\alpha h_i(t)/2. \tag{7}$$

In Eq. (5), the operators "+" and "−" correspond to counter- and co-propagation, respectively. To solve the equations, we substitute the form of a traveling wave for the instant SOA gain coefficient, i.e., $g(z,t) = g(t - z/v_{SOA})$.

In case of TPMZ, the control pulse and the probe clock co-propagate along the SOA at the same speed. Thus the effect of the control pulse on the probe clock seems stationary. Accordingly, the integral for Eq. (5) reduces to the simple form of Eq. (8)

$$h_i(t) = g_i(t)L. \tag{8}$$

In case of CPMZ, the counter-propagation integral is more complicated in Eq. (9), since the shape of the instant gain coefficient varies with the SOA length when the control pulse and the probe clock travel past each other in the SOA

$$h_i(t) = \frac{1}{L}\int_{-L/2}^{L/2} \ln G_i(t - 2zn_{SOA}/c)\,dz. \tag{9}$$

The intensity transmission characteristics at Ports 3 and 4 of the XOR gate can be expressed as:

$$T_3(t) = \frac{1}{4}G_1(t)\Big\{k_1k_2 + (1-k_1)(1-k_2)R_G - 2\sqrt{k_1k_2(1-k_1)(1-k_2)R_G} \times \cos[\Delta\phi_1(t) - \Delta\phi_2(t)]\Big\}, \tag{10}$$

$$T_4(t) = \frac{1}{4}G_1(t)\Big\{k_1(1-k_2) + (1-k_1)k_2R_G + 2\sqrt{k_1k_2(1-k_1)(1-k_2)R_G} \times \cos[\Delta\phi_1(t) - \Delta\phi_2(t)]\Big\}, \tag{11}$$

where $R_G = G_2(t)/G_1(t)$, k_1 and k_2 are the ratios of couplers C1 and C2, respectively. For simplicity, we set $k_1 = k_2 = 0.5$ in this paper. Thus, the output signal power at Ports 3 and 4 can be obtained as

$$P_j(t) = P_{PRB}(t)T_j(t), \quad j = 3, 4, \tag{12}$$

where $P_{PRB}(t)$ is the power of the probe signal.

3. Simulations and results

To analyze and optimize the gate performance, we conduct numerical simulations, where both input logic signals are 20 or 40 Gb/s RZ pseudo-random bit sequences (PRBS) with the word length of 2^7–1. During the fitting procedure, iterative method is used to solve such a large space of parameters. At first, some parameters are treated as constants of representative values for InGaAsP semiconductor materials operating at a wavelength of approximately 1.55 μm, as listed in Table 1. Then, some reasonable guess is made for the scopes of key SOA parameters that exert influence on the

中国科技论文在线 http://www.paper.edu.cn

Table 1
Description and values of some fixed parameters in first-step fitting procedure

Description	Value
Effective index of SOA	$n_{SOA} = 3.22$
Nonlinear gain compression factor	$\varepsilon = 0.31\ W^{-1}$
General gain factor	$a_N = 2.5 \times 10^{-20}\ m^{-3}$
SOA effective active area	$d \cdot W = 0.6 \times 1.5\ \mu m^2$
Contrast ratio of input signal	30 dB
Control pulse center wavelength	$\lambda_{CTRL} = 1.546\ \mu m$
Control pulse-width	$T_{CTRL} = 5$ ps
Control pulse energy	$E_{CTRL} = 250$ fJ
Probe pulse center wavelength	$\lambda_{PRB} = 1.56\ \mu m$
Probe pulse-width	$T_{PRB} = 5$ ps
Probe pulse energy	$E_{PRB} = 3$ fJ

gate performance. These parameters include τ_C, α, Γ, L, g_0, E_{sat}, and so on. Equations are solved using the initial guess to give an approximate solution. Thereafter, we adjust these values within reasonable limits in the next iterations to search for improved approximation, with respect to the optical signal parameters, such as the input pulse energy and the pulse-width. Instead of the maximum differential phase-shift ($\max|\Delta\phi_1 - \Delta\phi_2|$), we select the output contrast ratio (CR) as the optimization criteria, which indicates the opening of the eye diagram and is defined as the ratio of minimum output peak power for ONE to maximum output peak power for ZERO in decibel.

To start, we study the SOA parameters for XOR gate operating at 20 Gb/s, with the optical signal parameters fixed. Under pseudorandom input signals, we plot CR against L for both TMZI and CMZI, with τ_C as a parameter, as shown in Fig. 2(a). No wonder, shorter L and τ_C may yield better gate performance. According to the slopes of CR, the SOA length effect on CMZI is obviously stronger than that on TMZI, since in CMZI the gain coefficient may vary at different points of the SOAs. As a result, CR for CMZI drops apparently with the increase of the SOA length, while it for TMZI remains almost the same. With the other parameters fixed as in Fig. 2(a), to obtain a CR over 8 dB for 20 Gb/s operation, L and τ_C should be less than 250 μm and 150 ps, respectively.

Thereafter, setting $L = 100$ μm and $\tau_C = 100$ ps, we go on study the influence by Γ and α on the CMZI-based XOR gate performance, as shown in

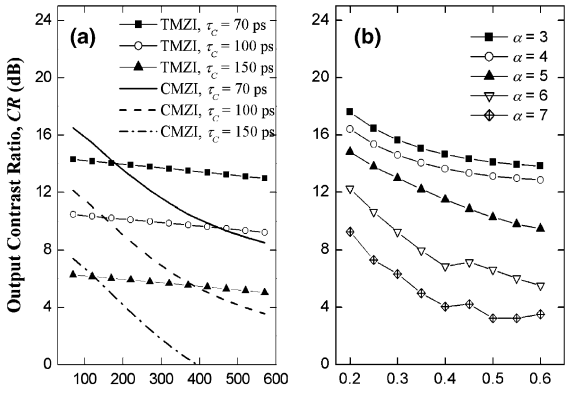


Fig. 2. Output contrast ratio for 20 Gb/s XOR operation under pseudorandom input signals: (a) CR vs. L for both TMZI and CMZI, with τ_C as a parameter, $g_0 = 25$ dB, $\Gamma = 0.39$ and $\alpha = 3$; (b) CR vs. Γ for CMZI, with α as a parameter, $g_0 = 25$ dB, $\tau_C = 100$ ps and $L = 100$ μm.

Fig. 2(b). CR degrades sharply when Γ or α increases. To get a CR for over 8 dB for 20 Gb/s operation, these two parameters are expected to be below 0.5 and 5, respectively.

Similar observation for 40 Gb/s operation has been captured in Fig. 3(a), where the limits to parameters become tighter, e.g., $\Gamma < 0.35$ and $\alpha < 4$ to reach a CR over 8 dB for a 40 Gb/s XOR gate under given conditions. Fig. 3(b) illustrates the relationship between α and the gate's switching

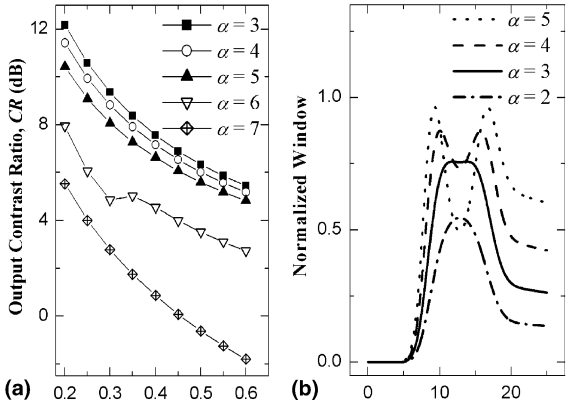


Fig. 3. Output contrast ratio and normalized switching window of the XOR gate operating at 40 Gb/s: (a) CR vs. Γ for CMZI, with α as a parameter, $g_0 = 25$ dB, $\tau_C = 100$ ps and $L = 100$ μm; (b) evolution of the normalized switching window with α, for CMZI, $g_0 = 25$ dB, $\tau_C = 100$ ps, $L = 150$ μm and $\Gamma = 0.3$.

中国科技论文在线 http://www.paper.edu.cn

window. In accordance with Eq. (7), the larger the α is, the sharper the phase will shift and, consequently, the higher the window will open. However, when $\alpha > 4$, the window becomes distorted and broadened severely, and thus serious trailing-edge intersymbol interference (ISI) deteriorates the gate performance.

The SOA saturation power (P_{sat}) is also among key parameters of the XOR gate. Although most of the factors related to P_{sat} have been analyzed in the above, we still give a direct view of the relationship between P_{sat} and CR in Fig. 4, where CR increases almost linearly with P_{sat}. To obtain a CR over 8 dB, P_{sat} should exceed only 5 pJ for 20 Gb/s operation, but 11 pJ for 40 Gb/s operation. To keep P_{sat} exceeding 11 pJ, a large SOA active area ($d \cdot W$) and a small confinement factor (Γ) are expected. The knot is that Γ usually drops with the increase of d. However, for reason of single-mode operation, d should not increase too much and must satisfy $d < \lambda_0/2(n_{SOA}^2 - n_2^2)^{1/2}$. To address this problem, many studies have been made, such as the multi-waveguide SOA [14].

Feeling partially confident of these SOA parameters, we select the moderate values of them within the above-desirable scopes and simulate the dynamic gains and phases of the XOR gate operating at 40 Gb/s. A portion of simulated phase changes in both arms of CMZI and the differential phase-shift ($\Delta\phi_1 - \Delta\phi_2$) are shown in Fig. 5. The corresponding input and output signals are shown in Fig. 6, which conveys the XOR truth-table is realized desirably through SOA-based CMZI operating at 40 Gb/s. The extinction ratio of the output signal is around 9.22 dB.

This portion of simulation results is selected on purpose, which contains continuous ONE bits to show apparent bit-pattern effect of the gate. As shown in Fig. 5, during each ONE bit-period, the SOA gain toboggans and the probe pulse

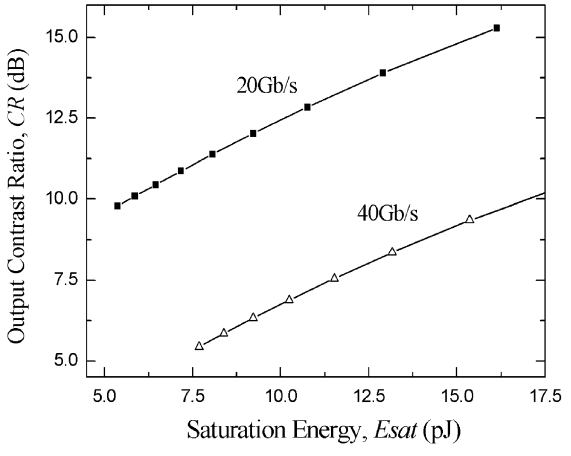


Fig. 4. Output contrast ratio vs. SOA saturation energy, $g_0 = 25$ dB, $\Gamma = 0.39$, $\tau_C = 100$ ps, $L = 100$ μm and $\alpha = 3$.

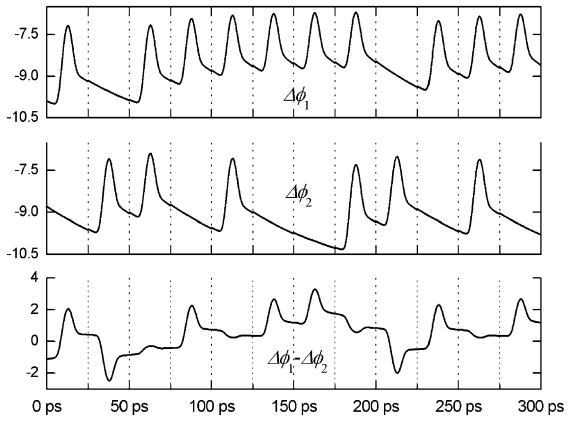


Fig. 5. Simulated phase changes of the probe pulses in both arms of CMZI and differential phase-shift between them, under 40 Gb/s pseudorandom input signals, $A = (1011111101110011)_2$, $B = (0110100110101101)_2$, $g_0 = 25$ dB, $\Gamma = 0.3$, $\tau_C = 100$ ps, $L = 100$ μm and $\alpha = 3$.

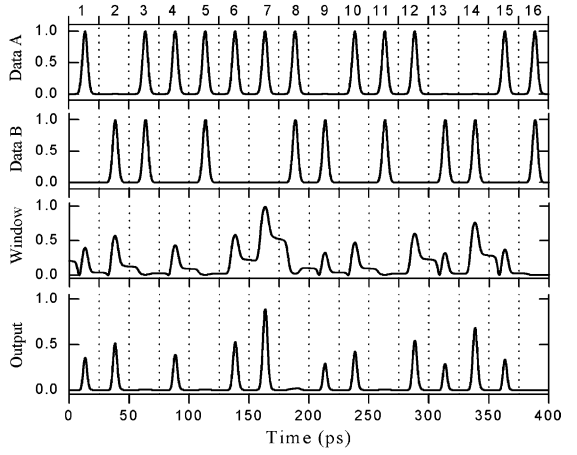


Fig. 6. Input logic signals and simulated output signals of CMZI, under 40 Gb/s pseudorandom input signals, $A = (1011111101110011)_2$, $B = (0110100110101101)_2$, $g_0 = 25$ dB, $\Gamma = 0.3$, $\tau_C = 100$ ps, $L = 100$ μm and $\alpha = 3$.

中国科技论文在线 http://www.paper.edu.cn

undergoes an abrupt phase change, while in each ZERO bit-period the gain recovers and the phase change levels gradually. Continuous ONE bits saturate the SOA further and continuous ZERO bits help the gain to rise further. That is why, during the sixth and 14th bit-periods, $\Delta\phi_1 - \Delta\phi_2$ is accumulated almost to its max ($\pm\pi$).

Correspondingly, the maximum differential phase-shift ($+\pi$) accounts for the most opened window and the highest output ONE bit in Fig. 7. To achieve an ideal interfering effect in CMZI, $\Delta\phi_1 - \Delta\phi_2$ should be $k\pi$, where k is an odd integer. However, to yield a satisfactory performance, $\Delta\phi_1 - \Delta\phi_2$ is unnecessary to be $k\pi$, because the interferometer, which is biased for a null, can switch well even if $|\Delta\phi_1 - \Delta\phi_2|$ is less than π. Therefore, good switching can be achieved with less pulse energy. Examples are shown in combination of Figs. 5 and 6, where $|\Delta\phi_1 - \Delta\phi_2| < \pi$ for most of the time, while *CR* still remains over 9 dB.

The output peak power uncertainty in Fig. 6 reveals the bit-pattern dependence of the XOR gate, ascribed mainly to the advent of continuous ONE bits. Due to the saturation in SOA and the slow gain recovery, when *A* and *B* are identical, the gate window will close to some extent but not completely, which induces inter-symbol crosstalk onto the output signal. An example is shown during the eighth bit-period. Although *A* and *B* are both ONE, SOA1 is in deep saturation after continuous ONE bits while SOA2 in relatively shallow saturation. Thus the gate window does not close completely and accounts for the maximum peak power for ZERO bit.

Through simulations with various parameters, we find that larger τ_C, α and ε may slower the falling edge of the window, or result in a minor window right after the major one, and thus introduce serious ISI. Designing a longer SOA length properly may lower the minor window and suppress the crosstalk, however, at the cost of time delay, power penalty and thus the performance degradation.

The window-width is an important factor to limit the gate operating speed. We study the window-width with various SOA parameters, among which we find the most effective ones are g_0 and τ_C, as shown in Fig. 7. The 3 dB window-width extends evidently with the increase of these two parameters. When 3 dB window-width exceeds 10 ps, it is almost impossible for the gate to operate at 40 Gb/s. Consequently, it is necessary to satisfy $g_0 < 25$ dB and $\tau_C < 150$ ps for 40 Gb/s operation with acceptable performance.

Assigning moderate values to SOA parameters within reasonable limits, we study the gate performance with respect to the optical signal parameters, such as the input pulse energy and the pulse-width. There is no wonder that shorter pulse-width is preferable to improve the XOR operation for both TMZI and CMZI. As revealed in Fig. 8, for 20 Gb/s operation, the pulse-width

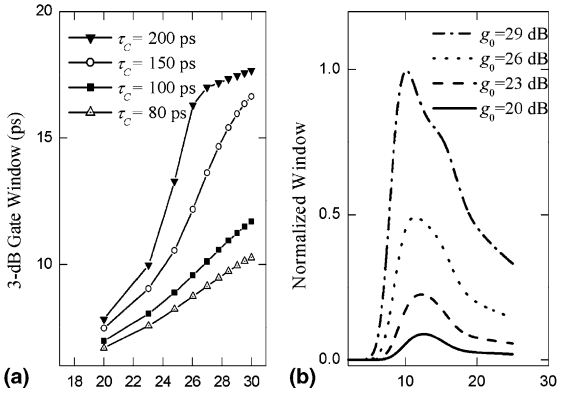


Fig. 7. Evolution of the normalized switching window with small signal gain (g_0) for CMZI, $\tau_C = 100$ ps, $L = 150$ μm, $\alpha = 3$ and $\Gamma = 0.3$.

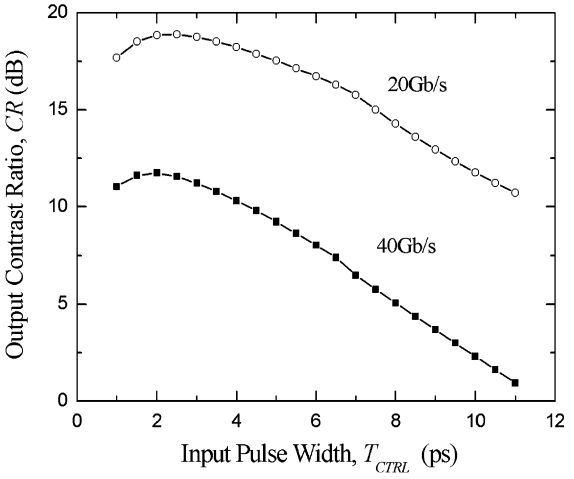


Fig. 8. Output contrast ratio vs. control pulse-width for CMZI, with signal rate as a parameter, $g_0 = 25$ dB, $\Gamma = 0.3$, $\tau_C = 100$ ps, $L = 100$ μm, $\alpha = 3$ and $E_{CTRL} = 250$ fJ.

中国科技论文在线 http://www.paper.edu.cn

can extends to more than 12 ps while the *CR* over 10 dB is maintained. For 40 Gb/s operation, when the control or the probe pulse-width exceeds 10 ps, the gate window will close completely under given conditions. Another phenomenon is that the gate performance begins to degenerate when pulse-width <2 ps, for reason of a secondary switching window due to the intra-band process.

The probe pulse energy should be too small to modify the optical properties of the SOA. Fixing the values of the other parameters, we enhance the control pulse energy (E_{CTRL}) gradually and examine the output signals. When E_{CTRL} exceeds a certain value, e.g., 0.4 pJ in Fig. 9, the improvement by enhancing E_{CTRL} becomes inapparent.

According to the above discussion, we state some rules regarding the influence by key parameters and the choice of them.

1. Shorter L may yield better gate performance; moreover, the length effect on CMZI is obviously stronger than that on TMZI.
2. Larger g_0, smaller Γ, ε, τ_C and α all lead to a high *CR*; generally, *CR* increases almost linearly with P_{sat}.
3. Shorter pulse-width is preferable to improve the XOR operation for both TMZI and CMZI; however, the performance of CMZI gate begins to degenerate when pulse-width <2 ps, due to the appearance of a secondary switching window.
4. The improvement by enhancing E_{CTRL} is relatively inapparent.
5. To yield a satisfactory performance, a differential phase shift of $k\pi$ is unnecessary; therefore, good switching can be achieved with less pulse energy than ideally needed.
6. The bit-pattern effect appears more seriously with the advent of continuous incoming ONE bits.
7. Larger τ_C and small g_0 may slower the falling edge of the window, and large α may result in a secondary switching window, all of which will introduce serious trailing-edge ISI, aggravate the pattern dependence and thus limit the operation speed.
8. With values of the other factors fixed, to get a *CR* over 8 dB, the parameter scopes for 20 Gb/s XOR operation are $L < 250$ μm, $\tau_C < 150$ ps, $\Gamma < 0.5$, $\alpha < 5$ and $P_{sat} > 5$ pJ; the scopes become tighter for 40 Gb/s operation, i.e., $L < 250$ μm, $\tau_C < 100$ ps, $\Gamma < 0.35$, $\alpha < 4$, $P_{sat} > 11$ pJ, $g_0 > 25$ dB, $E_{CTRL} > 0.15$ pJ and pulse-width <6 ps.

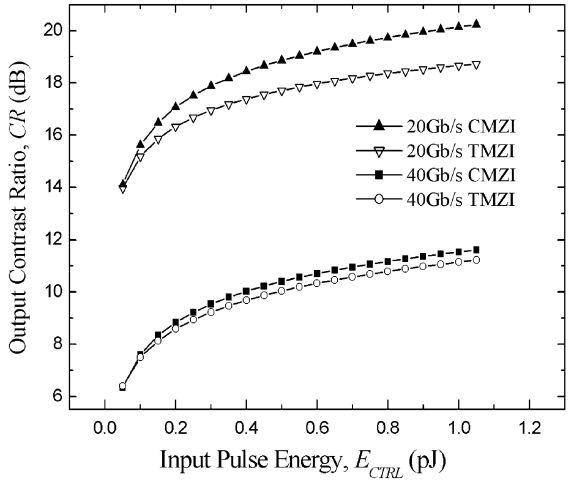


Fig. 9. Output contrast ratio (*CR*) vs. input control pulse energy for both TMZI and CMZI, with signal rate as a parameter, $g_0 = 25$ dB, $\Gamma = 0.3$, $\tau_C = 100$ ps, $L = 100$ μm, $\alpha = 3$ and $T_{CTRL} = 5$ ps.

4. Conclusions

We have analyzed the performance of SOA-MZI-based XOR gate through numerical simulations, in searching of the optimal parameters as well as the suitable operation condition. Several rules and limits on the parameter design have been stated. With properly designed parameters, the ultra-fast all-optical XOR gate can be realized with fairly high performance using SOA-MZI. Generally, the optimal values of these key parameters are not unique and should be determined in a comprehensive way.

We have to point out that the results of our preliminary work give an approximate solution to the ultra-fast XOR gate design. The influence on the XOR gate by pulse wavelength is not studied separately in this paper, which is more complicated since the wavelength correlates with many SOA parameters. With consideration of ASE, the scopes of key parameters will be tighter. Finally,

中国科技论文在线 http://www.paper.edu.cn

if the control pulse energy exceeds 1 pJ, the effects of TPA and UNR should be taken into account.

Acknowledgements

This study is supported by National Science Foundation of China (Project: ''Research on Key Technologies of Tbit/s Optical Packet Switching''). We would like to express our appreciation to Prof. Dr. Wolfgang Schleich and the two anonymous reviewers for their constructive comments and helpful suggestions.

References

[1] T.J. Xia, Y. Liang, K.H. Ahu, J.W. Lou, O. Boyraz, Y.-H. Kao, X.D. Cao, S. Chaikamnerd, J.K. Anderson, M.N. Islam, IEEE Photon. Technol. Lett. 10 (1998) 153.
[2] A.J. Poustie, K.J. Blow, A.E. Kelly, R.J. Manning, Opt. Commun. 156 (1998) 22.
[3] T. Houbavlis, K. Zoiros, A. Hatziefremidis, et al., Electron. Lett. 35 (1999) 1650.
[4] G. Theophilopoulos, K. Yiannopoulos, M. Kalyvas, C. Bintjas, G. Kalogerakis, H. Avramopoulos, L. Occhi, L. Schares, G. Guekos, S. Hansmann, R. Dall'Ara, OFC 2001, vol. 1, 2001, MB2/1.
[5] T. Fjelde, D. Wolfson, A. Kloch, B. Dagens, A. Coquelin, I. Guillemot, F. Gaborit, F. Poingt, M. Renaud, Electron. Lett. 36 (2000) 1863.
[6] H.K. Jae, M.J. Young, T.B. Young, IEEE Photon. Technol. Lett. 14 (2002) 1436.
[7] D. Chiaroni, B. Lavigne, Proc. Postdeadline ECOC'97 5 (1997) 41.
[8] G. Pagrawal, N.A. Olsson, IEEE J. Quantum Electron. 25 (1989) 2297.
[9] A. Mecozzi, J. Mork, J. Opt. Soc. Am. B 14 (1997) 761.
[10] J.M. Tang, K.A. Shore, IEEE J. Quantum Electron. 34 (1998) 1263.
[11] J.M. Tang, P.S. Spencer, K.A. Shore, IEEE J. Lightwave Technol. 16 (1998) 86.
[12] M.G. Kane, I. Glesk, J.P. Scokoloff, P.R. Prucnal, Appl. Opt. 33 (1994) 6833.
[13] K.I. Kang, T.G. Chang, I. Glesk, P.R. Prucnal, Appl. Opt. 35 (1996) 417.
[14] B. Dagens, J.Y. Emergy, C. Janz, Electron. Lett. 35 (1999) 485.